

Nucleation mechanisms and the elimination of misfit dislocations at mismatched interfaces by reduction in growth area

E. A. Fitzgerald,^{a)} G. P. Watson, R. E. Proano, and D. G. Ast
Department of Materials Science and Engineering, Cornell University, Ithaca, New York 14853

P. D. Kirchner, G. D. Pettit, and J. M. Woodall
IBM T. J. Watson Research Center, Yorktown Heights, New York 10598

(Received 15 August 1988; accepted for publication 18 November 1988)

To investigate the effect of growth area on interface dislocation density in strained-layer epitaxy, we have fabricated 2- μm -high mesas of varying lateral dimensions and geometry in (001) GaAs substrates with dislocation densities of 1.5×10^5 , 10^4 , and 10^2 cm^{-2} . 3500-, 7000-, and 8250- \AA -thick $\text{In}_{0.05}\text{Ga}_{0.95}\text{As}$ layers, corresponding to 5, 10, and 11 times the experimental critical layer thickness as measured for large-area samples, were then deposited by molecular-beam epitaxy. For the 3500- \AA layers, the linear interface dislocation density, defined as the inverse of the average dislocation spacing, was reduced from greater than 5000 to less than 800 cm^{-1} for mesas as large as 100 μm . A pronounced difference in the linear interface dislocation densities along the two interface $\langle 110 \rangle$ directions indicates that α dislocations nucleate about twice as much as β dislocations. For samples grown on the highest dislocation density substrates, the linear interface-dislocation density was found to vary linearly with mesa width and to extrapolate to a zero linear interface-dislocation density for a mesa width of zero. This behavior excludes dislocation multiplication or the nucleation of surface half-loops as operative nucleation sources for misfit dislocations in these layers. Only nucleation sources that scale with area (termed fixed sources) are active. In specimens with lower substrate dislocation densities, the density of interface dislocations still varies linearly with mesa size, but the slope becomes independent of substrate dislocation density, indicating that surface inhomogeneities now act as the dominant source for misfit dislocations. Thus, in 3500- \AA -thick overlayers, substrate dislocations and substrate inhomogeneities are the active fixed nucleation sources. Since only fixed nucleation sources are active, a single strained layer will dramatically reduce the threading dislocation density in the epilayer. For the 7000- \AA layers, we observe a superlinear increase in linear interface-dislocation density with mesa size for mesas greater than 200 μm , indicating that dislocation multiplication occurs in large mesas. For mesas less than 200 μm in width, linear interface-dislocation density decreases linearly with mesa size, but extrapolates to a nonzero linear interface-dislocation density for a mesa size of zero. This nonzero extrapolation suggests an additional active source which generates a dislocation density that cannot be decreased to zero by decreasing the mesa size. Cathodoluminescence (CL) images using radiative recombination indicate that the additional source is nucleation from the mesa edges. Despite a doubling in epilayer thickness from 3500 to 7000 \AA , the linear interface-dislocation density for mesas 100 μm in width is still very low, approximately 1500 cm^{-1} . The 8250- \AA layers possess interface-dislocation densities too high to be accurately determined with CL. However, increases in CL intensity as mesa width is reduced indicate that the interface-dislocation density is decreasing and that growth on small areas produces higher-quality layers than growth on large areas. Our investigations show that different sources for misfit dislocations become active at different epilayer strain levels. The critical thickness depends on which type of nucleation source becomes activated first; therefore, different critical thicknesses can be observed depending on which kind of source is present in a specimen.

I. INTRODUCTION

Lattice-matched systems are used to fabricate most heterostructure devices since lattice matching eliminates misfit dislocations which form at mismatched interfaces. However, relatively few lattice-matched systems with large band offsets exist, limiting the design options for novel electrical and optical devices. If defect-free growth can be extended to lattice-mismatched systems, a much wider selection of band

gaps and band offsets would be available, leading to the improvement of existing devices and the construction of novel ones.

Lattice-mismatched systems have been investigated for a variety of devices.¹⁻⁵ In many of these applications, mildly lattice-mismatched systems are used and the epilayer thicknesses are kept below the critical thickness for defect formation (these totally elastically strained layers are termed pseudomorphic).^{1,6} Extension of the pseudomorphic approach to layers with larger lattice mismatch and thicker epilayers is of considerable technological interest.

^{a)} Present address: AT&T Bell Laboratories, 600 Mountain Avenue, Murray Hill, NJ 07974-2070.

Despite the continued interest in mismatched semiconductor systems, the nucleation mechanisms for misfit dislocations are still relatively unexplored. Most studies of misfit dislocation formation are based on post-growth observations, and the origin of misfit dislocations must therefore be deduced from dislocation structure and the thickness at which dislocations are first observed,⁷⁻⁹ often called the critical thickness. But the criterion of critical thickness is a vague one, due to the varying ability of different measurements to detect the onset of misfit dislocation formation,¹⁰ the metastable nature of the epilayers from different systems, and comparison with incorrect theoretical critical thickness expressions.¹¹

If experimental results are compared with the correct expression for the critical thickness first proposed by Matthews *et al.*,¹² the metastable nature of the films becomes apparent since the experimental critical thicknesses are greater than Matthews' theoretical critical thickness,^{11,13} especially when the mismatch is less than 2%. A consequence of this metastability due to the kinetics of misfit dislocation formation is that the interface-dislocation density depends on the size of the growth area. It has recently been shown that by reducing the growth area on the substrate before the mismatched semiconductor is deposited, one can reduce the number of, or even eliminate, misfit dislocations at mismatched $\text{In}_{0.05}\text{Ga}_{0.95}\text{As}/(001)\text{GaAs}$ (mismatch approximately 0.4%) heterostructure interfaces.¹⁴ Technologically, these results make possible a number of previously unattainable devices. Scientifically, they demonstrate that growth area is a variable which can be used to study and determine mechanisms of misfit dislocation nucleation.

In this paper, we report on the interface structure of nominally $\text{In}_{0.05}\text{Ga}_{0.95}\text{As}/(001)\text{GaAs}$ heterostructures grown on patterned substrates containing many mesas, varying in lateral dimensions and geometry. By using CL to observe linear interface-dislocation densities as a function of mesa size, we are able to deduce which nucleation mechanisms are active for different epilayer thicknesses. We have observed interface-dislocation densities near zero for epilayers grown at approximately 10 times the experimental critical layer thickness as estimated in large areas.

II. EXPERIMENTAL PROCEDURE

To observe the effects of area on interface-dislocation density, we fabricated 2- μm -high mesas with a variety of shapes in (001) GaAs substrates with dislocation densities of 1.5×10^5 , 10^4 , and 10^2 cm^{-2} using two different fabrication processes. One was a lift-off procedure described previously.¹⁴ In the other procedure, GaAs wafers were first coated with $\approx 3000\text{ \AA}$ of SiO_2 by chemical vapor deposition. After applying and patterning the photoresist, the SiO_2 was removed using reactive ion etching. After stripping the photoresist, the SiO_2 pattern was used as a mask for chemically assisted ion beam etching. 2 μm of GaAs was removed, resulting in mesas with vertical walls. The SiO_2 was left as a protective layer on the mesa tops, and was removed just prior to the molecular-beam epitaxial growth (MBE) using a HF and water solution. A 1500- \AA GaAs buffer layer was then deposited by MBE on the patterned substrate, followed

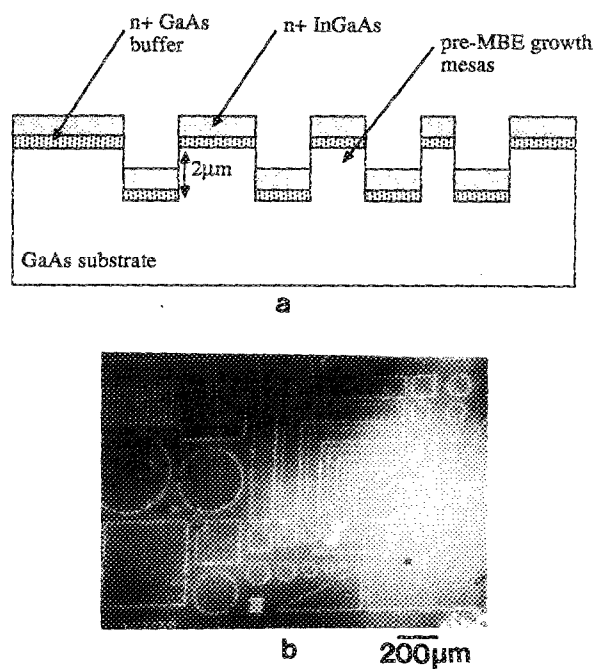


FIG. 1. (a) A schematic cross-sectional view of the mesa structures; (b) a plan-view SEM image of the mesa structures.

by either 3500, 7000, or 8250 \AA of nominally $\text{In}_{0.05}\text{Ga}_{0.95}\text{As}$.

As will be discussed later in this paper, 5% In was chosen so that a mismatch of 0.4% exists in the heterostructure, well below our estimates of the strain level necessary for the nucleation of dislocation half-loops from the surface.

Figure 1(a) is a schematic of the sample cross section, and Fig. 1(b) is a plan-view scanning electron microscope (SEM) image of the etch pattern which was repeated many times on a wafer. All layers were doped with Si to 10^{18} cm^{-3} to increase the intensity of the cathodoluminescence (CL) signal. The misfit dislocations at the heterointerface were observed in a JEOL JSM35CF SEM modified for CL with the addition of an annular photodiode¹⁵ and a monochromator-photomultiplier detection system.¹⁶ Typical operating conditions were an accelerating voltage of 10–17 keV and a beam current of 40–80 nA. Electron-beam x-ray analysis (wavelength dispersive spectroscopy), wavelength-sensitive CL, and Rutherford backscattering spectrometry (RBS) were used to confirm In composition and layer thicknesses.

TABLE I. Experimentally determined In compositions of the $\text{In}_x\text{Ga}_{1-x}\text{As}$ epilayers.

Thickness (\AA)	Dislocation density (cm^{-2})	x in $\text{In}_x\text{Ga}_{1-x}\text{As}$
3500	1.5×10^5	0.05
3500	10^4	0.075
3500	10^2	0.05
7000	1.5×10^5	0.05
7000	10^4	0.095
7000	10^2	0.05
8250	1.5×10^5	0.05

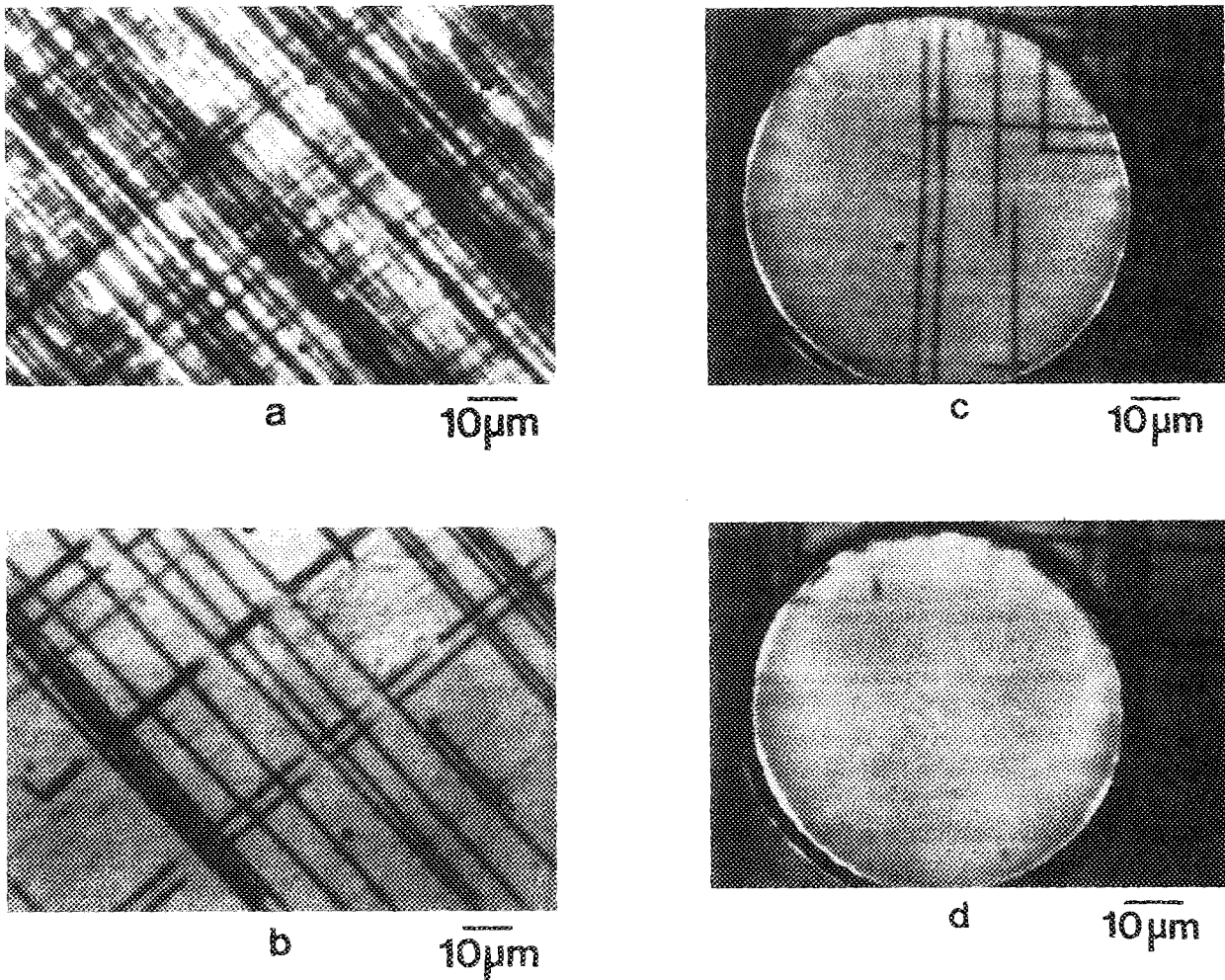


FIG. 2. CL images of the 3500-Å $\text{In}_{0.05}\text{Ga}_{0.95}\text{As}$ layer on the $1.5 \times 10^5 \text{ cm}^{-2}$ substrate: (a) large-area control sample; (b) 200- μm circular mesa; (c) 90- μm circular mesa; (d) 67- μm circular mesa.

Electron-beam x-ray analysis was also used to verify that the In composition was identical on different size mesas. The samples and their experimentally determined compositions are listed in Table I.

III. RESULTS

A. 3500-Å $\text{In}_{0.05}\text{Ga}_{0.95}\text{As}$

We first discuss the results obtained from 3500-Å-thick $\text{In}_{0.05}\text{Ga}_{0.95}\text{As}$ layers on GaAs substrates with grown-in dislocation densities of 1.5×10^5 , 10^4 , and 10^2 cm^{-2} . The epilayer thickness exceeds the critical thickness, as measured in a large area sample, by approximately a factor of 5. Figure 2(a) is a CL image of the control sample, 1 cm^{-2} in size and grown on a substrate with a dislocation density of $1.5 \times 10^5 \text{ cm}^{-2}$. Figure 3(a) is a CL image of a similar large-area control specimen grown on a substrate dislocation density of 10^4 cm^{-2} . The density of dislocations at the interface in these samples is so high that CL cannot be used to correctly determine the interface-dislocation density, since the dark line defects correspond to groups of dislocations.¹⁶⁻¹⁸ However, since overlap of CL dislocation images occurs for dislocation spacings of approximately less than 2 μm , we can

estimate that the linear dislocation density is greater than 5000 cm^{-1} .

We will first report the results from the circular mesas, followed by the square mesa results.

1. Circular mesas

Figures 2(b)–2(d) are planar CL images of the $\text{In}_{0.05}\text{Ga}_{0.95}\text{As}/\text{GaAs}$ interface on different size circular mesas. The substrate dislocation density was $1.5 \times 10^5 \text{ cm}^{-2}$. Figure 2(b) demonstrates that the linear interface-dislocation density in a 200- μm -wide circular mesa is dramatically lower than in the large-area sample [Fig. 2(a)]. Also note that a difference in linear interface-dislocation density exists along the two $\langle 110 \rangle$ directions. This difference in $\langle 110 \rangle$ dislocation densities is prominent in the 90- μm mesa structure as well [Fig. 2(c)], in which the interface-dislocation density has decreased even further. Figure 2(d) is a CL image of a nearly interface-dislocation-free, coherently strained epilayer on a 67- μm mesa.

Figures 3(b)–3(d) show CL images of overlayers on three different sized mesas fabricated in substrates with a substrate dislocation density of 10^4 cm^{-2} . As in Fig. 2, the

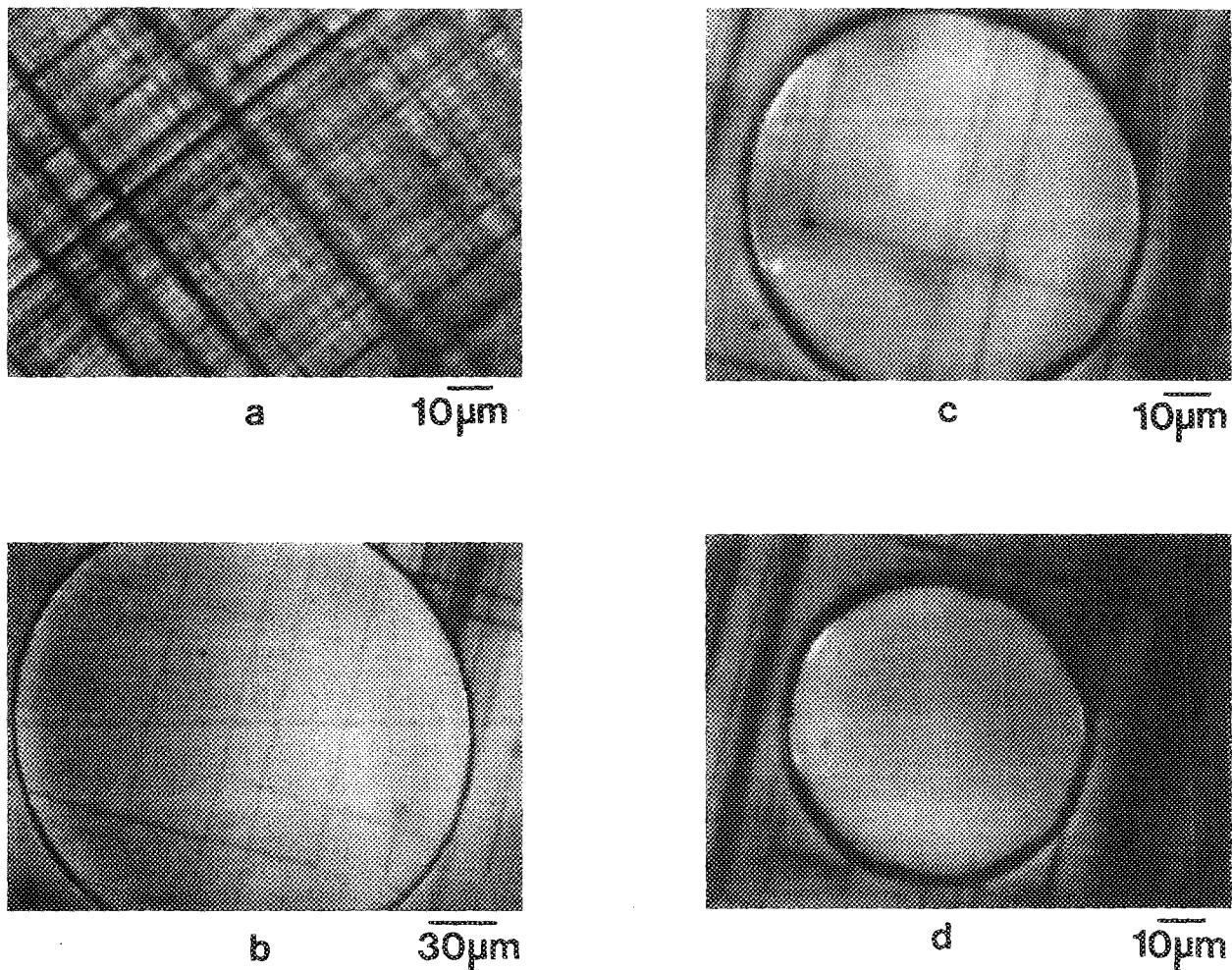


FIG. 3. CL images of the 3500-Å $\text{In}_{0.075}\text{Ga}_{0.925}\text{As}$ layer on the 10^4-cm^{-2} substrate: (a) large-area control sample; (b) 200- μm circular mesa; (c) 90- μm circular mesa; (d) 67- μm circular mesa.

interface-dislocation density decreases rapidly with mesa size in Figs. 3(b)–3(d), 200-, 90-, and 67- μm mesas, respectively. For comparison, we show in Fig. 3(a) a CL image from the large-area sample. Although the desired composition of the epilayer was 5%, we experimentally determined the actual composition with RBS to be $\text{In}_{0.075}\text{Ga}_{0.925}\text{As}$. Again, note the asymmetry in linear interface-dislocation densities across the two $\langle 110 \rangle$ directions. CL images of overlayers on mesas formed on the substrates with a dislocation density of 10^2 cm^{-2} are not shown, but their appearance was similar to those shown in Fig. 3.

Figures 2 and 3 qualitatively show the reduction in interface-dislocation density as the mesa size is reduced. However, to gain quantitative information and to discern differences due to different substrate dislocation densities, the linear interface-dislocation density was averaged over the many identical mesas on a wafer, and investigated as a function of mesa dimension and geometry. Due to the very low interface-dislocation densities in the mesas, the number of dislocations in many identical mesas, especially the smaller mesas, must be counted in order to arrive at statistically correct values.

We define linear interface-dislocation density as the average number of misfit dislocations crossed by a 1-cm-long line drawn perpendicular to the line direction of a set of parallel interface dislocations. In other words, the linear interface-dislocation density is the inverse of the average dislocation spacing and has units of cm^{-1} . It is important to note that the dislocation spacing, and therefore the linear interface-dislocation density, is different along the two different $\langle 110 \rangle$ directions.

The average linear interface-dislocation densities are plotted as a function of mesa diameter in Figs. 4(a)–4(c), which correspond to the samples with substrate dislocation densities of 1.5×10^5 , 10^4 , and 10^2 cm^{-2} . The following features are observed: (1) a decrease in linear interface-dislocation density with mesa size; (2) a difference in linear interface-dislocation densities along the two $\langle 110 \rangle$ directions; (3) linear fits through the data points; (4) extrapolations of the lines nearly through the origin; and (5) a large decrease in the slope of the linear fit with a decrease in substrate dislocation density as seen in comparing Figs. 4(a) and 4(b). The significance of these observations will be discussed in Sec. IV.

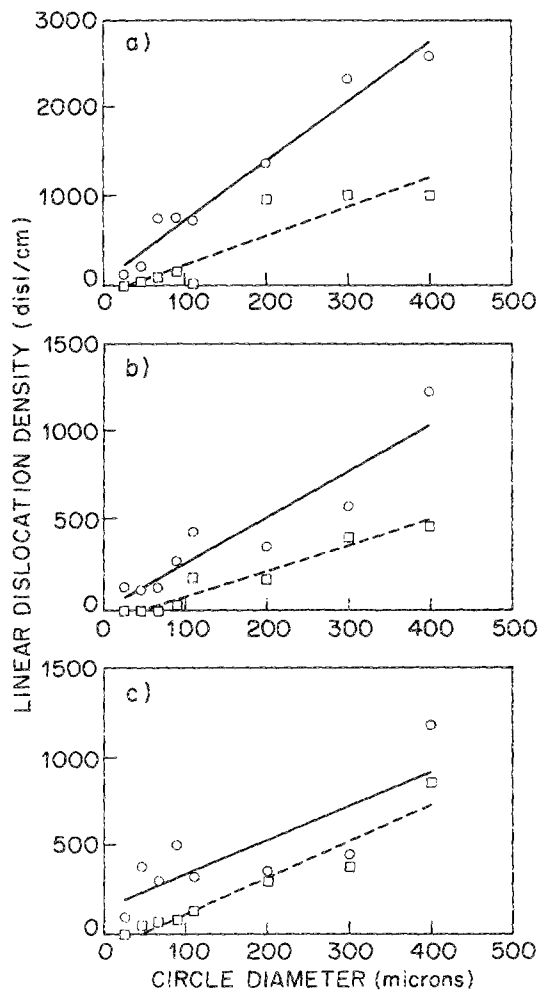


FIG. 4. Plots of average linear interface-dislocation density vs circular mesa diameter for the 3500-Å $\text{In}_{0.05}\text{Ga}_{0.95}\text{As}$ layers. The solid line represents the dense $\langle 110 \rangle$ direction (defined as $[110]$): (a) $1.5 \times 10^5 \text{ cm}^{-2}$ substrate; (b) 10^4 cm^{-2} substrate; (c) 10^2 cm^{-2} substrate.

2. Square mesas

The results obtained from square mesas covered with 3500-Å of $\text{In}_{0.05}\text{Ga}_{0.95}\text{As}$ are similar to those from the circular mesas. Figures 5(a)–5(d) show CL images of square mesas fabricated on a $1.5 \times 10^5 \text{ cm}^{-2}$ substrate. The square mesas in Fig. 5 are from the same sample as the circular mesas shown in Figs. 2(b)–2(d). The mesa sizes are 400, 200, 90, and $67 \mu\text{m}$. All square mesas were oriented such that their edges were parallel to $\langle 110 \rangle$ directions. Figures 6(a)–6(d) show identically sized square mesas on the 10^4 cm^{-2} substrate material. These mesas are from the same samples as the circular mesas in Figs. 3(b)–3(d). The CL images of square mesas on the 10^2 cm^{-2} substrate (not shown) were similar in appearance to those shown in Fig. 6.

As with the circular mesas, we average over a number of identically sized square mesas to create plots of linear interface-dislocation density versus square side length. Figures 7(a)–7(c) are plots using the data from samples with substrate dislocation densities of 1.5×10^5 , 10^4 , and 10^2 cm^{-2} , respectively. Observe that the results are very similar to

those for circular mesas and, with the exception of Fig. 7(a), the observations listed above for circular mesas hold for square mesas as well.

3. Miscellaneous observations

Figure 8 shows a low magnification CL image of mesas in a $1.5 \times 10^5 \text{ cm}^{-2}$ substrate covered with 3500 Å of $\text{In}_{0.05}\text{Ga}_{0.95}\text{As}$. Visible between the brighter, raised mesa structures is the CL image of the $\text{InGaAs}/\text{GaAs}$ interface in the valleys, which also show an altered dislocation density. For example, note that in the channel between the square mesas, dislocations predominately form along the unrestricted channel. Thus, lateral restriction by either walls or trenches will reduce the linear interface-dislocation density in the restricted direction. The high density of interface dislocations along the unrestricted $\langle 110 \rangle$ direction also suggests that the mean length of misfit dislocations is quite large, and that dislocation sources have a long-range effect.

Because of the difference in linear interface-dislocation densities along the two $\langle 110 \rangle$ interface directions, misfit dislocation nucleation can be substantially reduced by patterning in one direction only. Figure 9 is a CL image of a rectangular mesa oriented to block the dominant set of interface dislocations. The long side of the rectangle is aligned parallel to the misfit dislocations in the low dislocation density $\langle 110 \rangle$ direction. As Fig. 9 shows, blockage is not perfect, i.e., occasionally short segments cross the short dimension of the rectangle. Parallel to the long face, the interface-dislocation density is still near zero for most rectangular mesas except for the bottom mesa. CL images indicate that this mesa contains many process-induced surface inhomogeneities acting as nucleation sites.

The metastability of the highly strained films on the mesas is illustrated in Figs. 10(a)–10(c). Figure 10(a) is a CL image of a $110\text{-}\mu\text{m}$ -diam circular mesa. Defects visible as black dots clearly act as nucleation sites for misfit dislocations. Figure 10(b) is a SEM image corresponding to an area where a black dot was observed. The surface pit suggests that a particle or some other substrate surface inhomogeneity was responsible for the nucleation of a misfit dislocation. Figure 10(c) shows very large substrate surface debris due to the photoresist lift-off technique.¹⁴ Deposition over these areas resulted in the nucleation of a myriad of misfit dislocations, showing that, given sufficient dislocation nucleation sources, the film will relax by the creation of misfit dislocations.

B. 7000-Å $\text{In}_{0.05}\text{Ga}_{0.95}\text{As}$

We will now discuss the results obtained from 7000-Å-thick $\text{In}_{0.05}\text{Ga}_{0.95}\text{As}$ layers grown on GaAs substrates with dislocation densities of 1.5×10^5 , 10^4 , and 10^2 cm^{-2} . At this thickness, the epilayer exceeds the critical thickness, as measured in large-area samples, by approximately a factor of 10. Figure 11(a) is a CL image from the large-area control specimen grown on a substrate with a dislocation density of $1.5 \times 10^5 \text{ cm}^{-2}$. CL images of the control specimens with substrate dislocation densities of 10^4 and 10^2 cm^{-2} (not shown here) were similar to Fig. 11(a). As in the 3500-Å

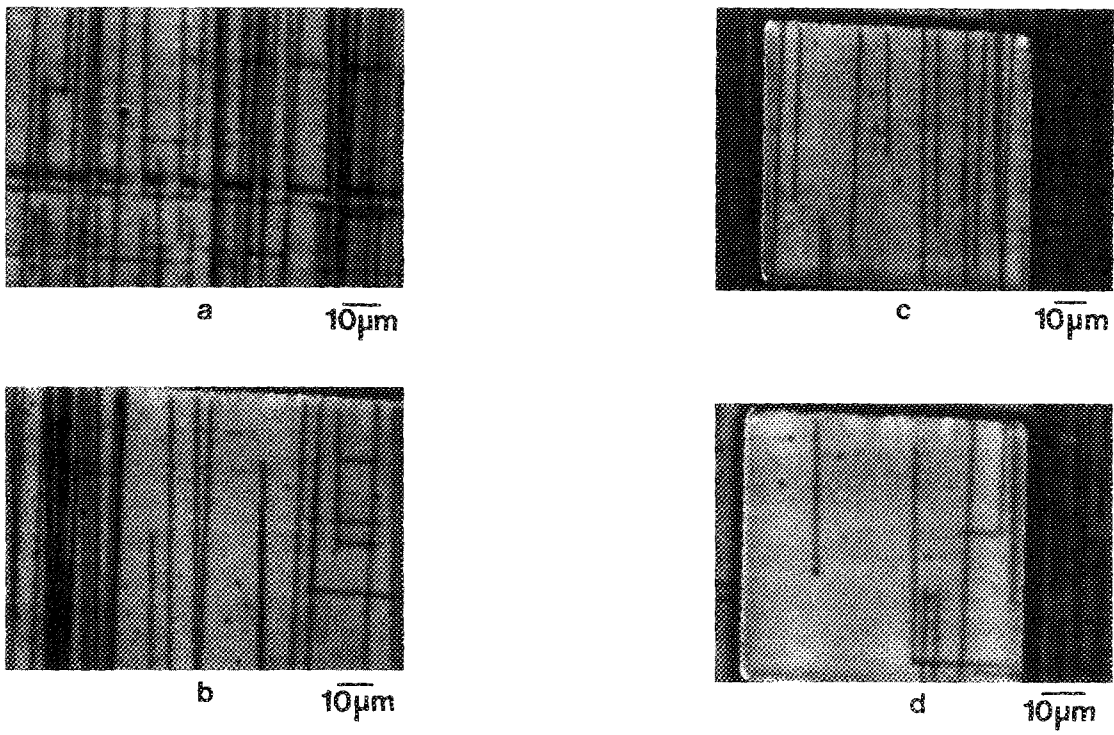


FIG. 5. CL images of the 3500-Å $\text{In}_{0.05}\text{Ga}_{0.95}\text{As}$ layer on the $1.5 \times 10^5\text{-cm}^{-2}$ substrate: (a) 400- μm square mesa; (b) 200- μm square mesa; (c) 90- μm square mesa; (d) 67- μm square mesa.

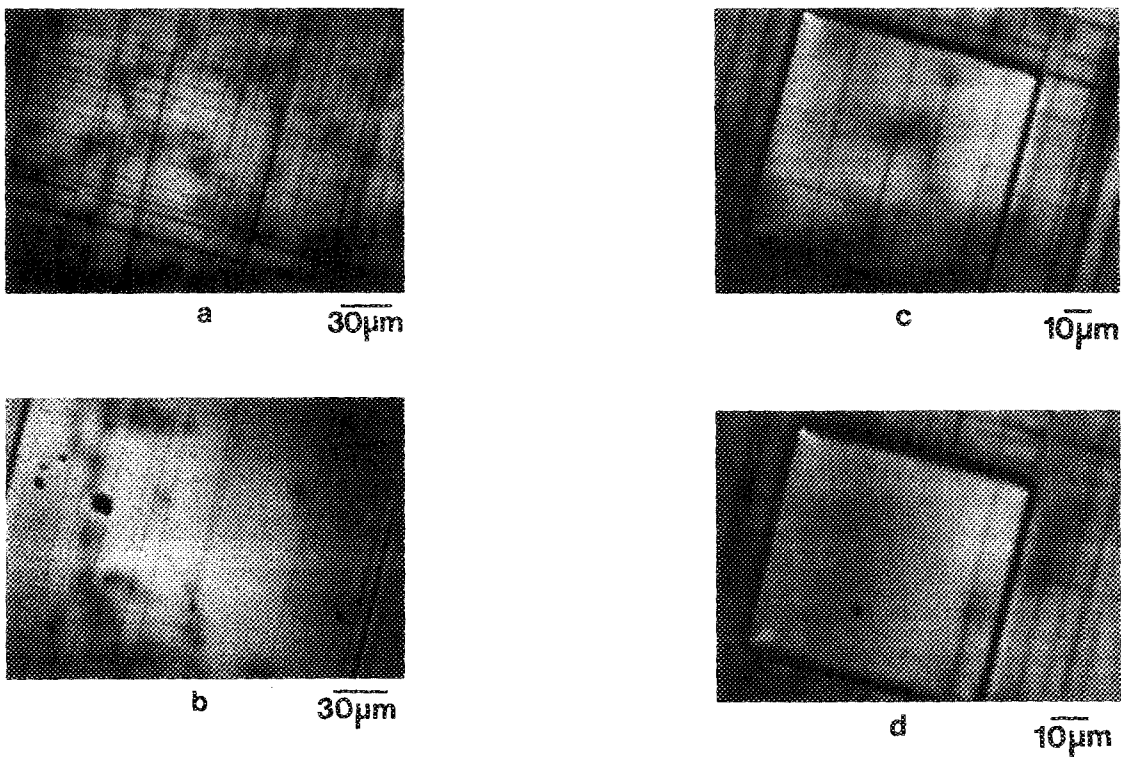


FIG. 6. CL images of the 3500-Å $\text{In}_{0.075}\text{Ga}_{0.925}\text{As}$ layer on the 10^4-cm^{-2} substrate: (a) 400- μm square mesa; (b) 200- μm square mesa; (c) 90- μm square mesa; (d) 67- μm square mesa.

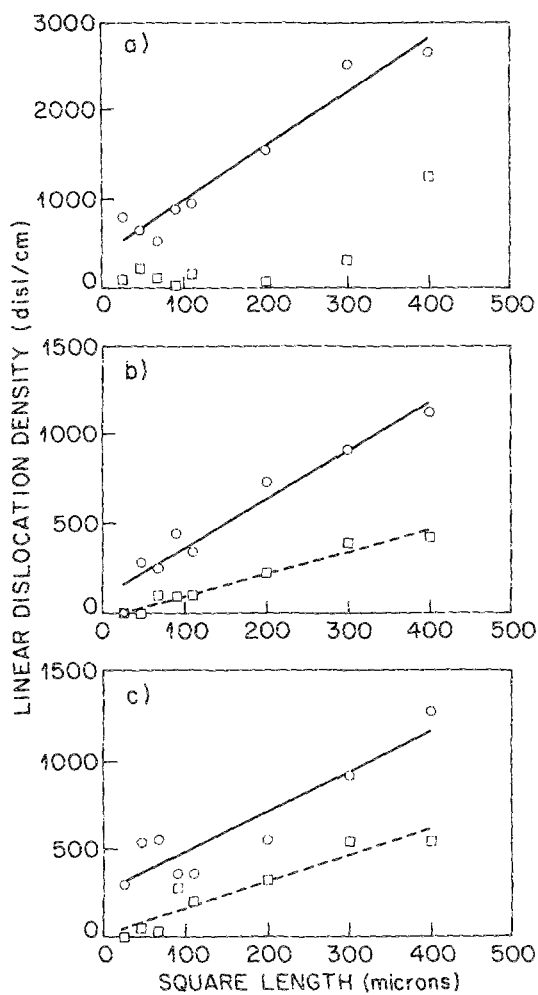


FIG. 7. Plots of average linear interface-dislocation density vs square mesa edge length for the 3500-Å $\approx \text{In}_{0.05}\text{Ga}_{0.95}\text{As}$ layers. The solid line represents the dense $\langle 110 \rangle$ direction (defined as $[110]$): (a) $1.5 \times 10^5\text{-cm}^{-2}$ substrate; (b) 10^4-cm^{-2} substrate; (c) 10^2-cm^{-2} substrate.

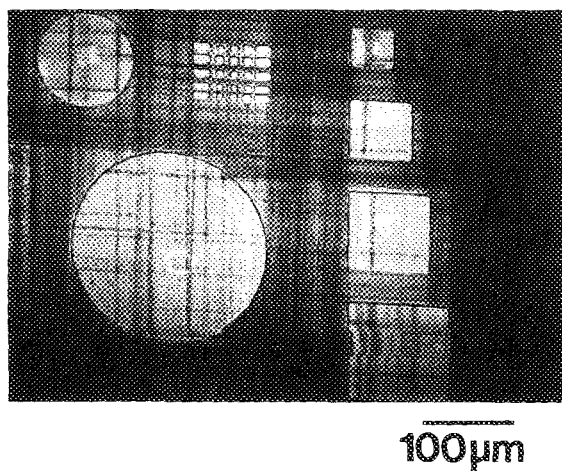


FIG. 8. CL image of a series of square islands which alter the interface-dislocation density in the interface between the mesas.

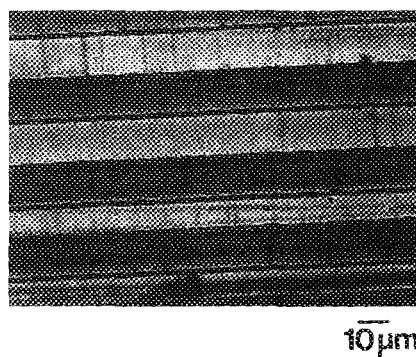


FIG. 9. Rectangular mesas, short side aligned with the easy (α) dislocation formation direction.

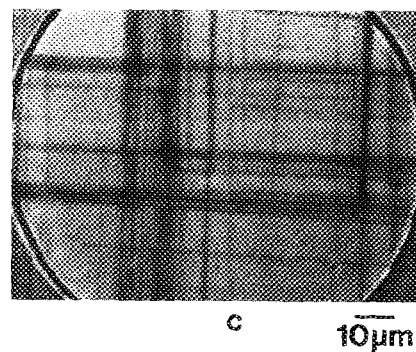
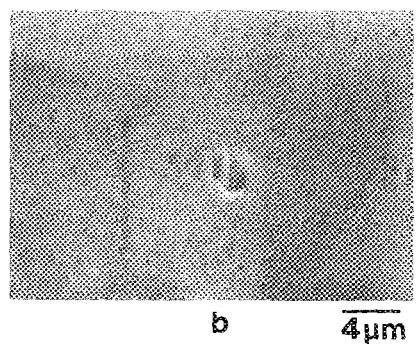
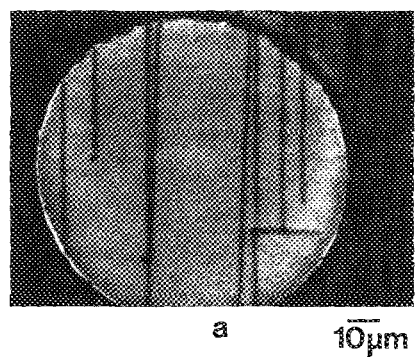


FIG. 10. Substrate surface inhomogeneities acting as nucleation sources: (a) CL image showing black dots which have nucleated misfit dislocations; (b) SEM image of the surface showing a pit corresponding to a black dot in CL; (c) CL image of substrate surface debris from the lift-off procedure which have nucleated many misfit dislocations.

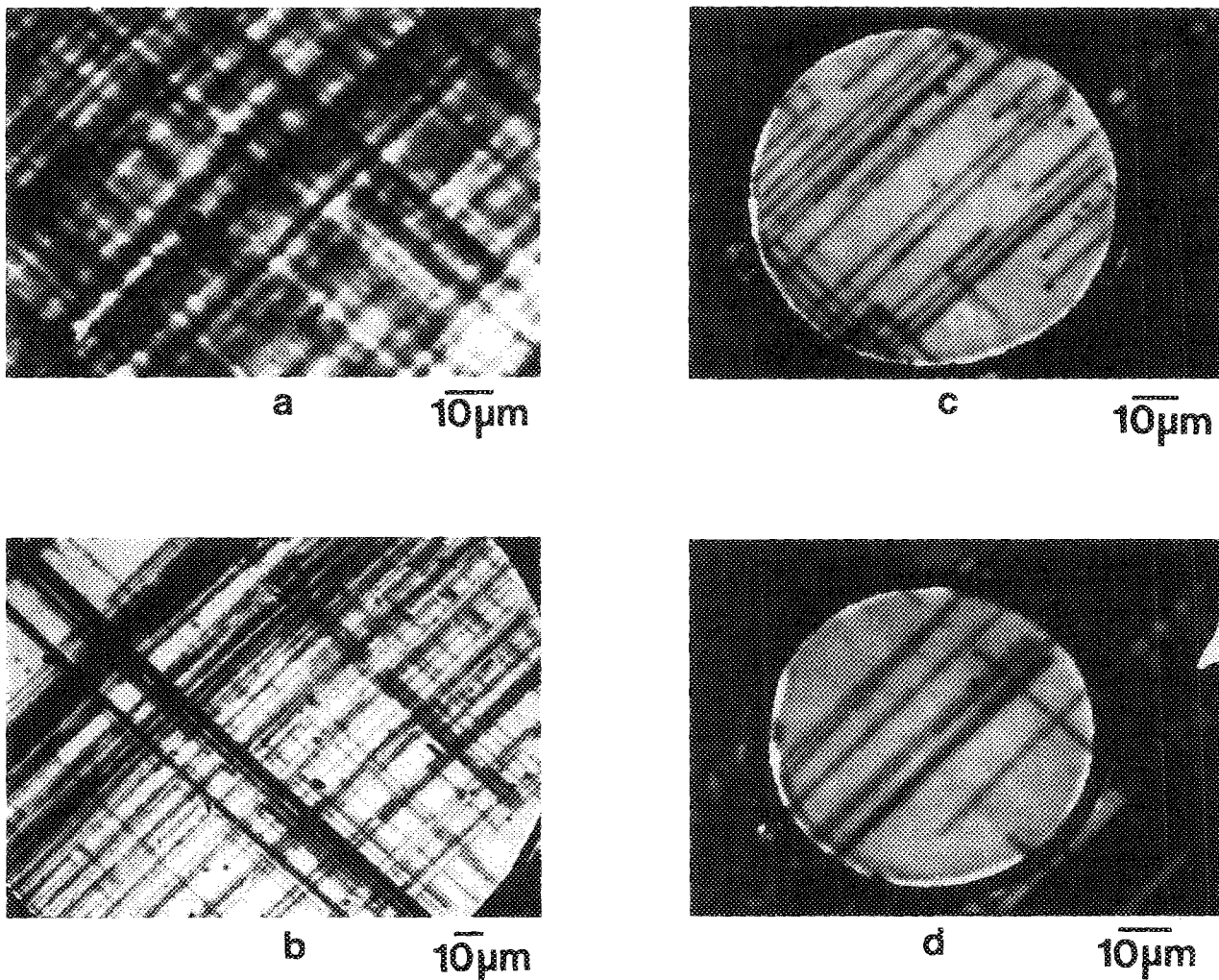


FIG. 11. CL images of the 7000-Å $\text{In}_{0.05}\text{Ga}_{0.95}\text{As}$ layer on the $1.5 \times 10^5\text{-cm}^{-2}$ substrate: (a) large-area control sample; (b) 200- μm circular mesa; (c) 90- μm circular mesa; (d) 67- μm circular mesa.

case, the large-area samples have an interface-dislocation density which is too high to be determined with CL.

As before, we will first report results obtained from the circular mesas, followed by those from the square mesas.

1. Circular mesas

Figures 11(b)–11(d) are CL images of 7000-Å $\text{In}_{0.05}\text{Ga}_{0.95}\text{As}$ grown on GaAs substrates with a dislocation density of $1.5 \times 10^5\text{ cm}^{-2}$. The mesa diameters are 200, 90, and 67 μm for Figs. 11(b)–11(d), respectively. Figure 11(b), the 200- μm mesa, exhibits a reduced interface-dislocation density relative to Fig. 11(a), but the density is still too high in some regions to permit accurate determination with CL. Also, dislocation bands from edge to edge are prominent in this mesa, indicating that heterogeneous misfit dislocation nucleation is active.

Figures 11(c) and 11(d) are CL images from 90- and 67- μm mesas. The interface-dislocation density has decreased to the point where dislocations can be accurately counted with CL. A large difference in dislocation densities

along the two $\langle 110 \rangle$ directions exists, as well as a large number of misfit dislocations extending from edge to edge across the mesa.

The CL images of the 7000-Å layers grown on the 10^4 - and 10^2-cm^{-2} substrates were similar to those in Fig. 11 and are not shown in Fig. 12.

Before analyzing the dislocation densities in 7000-Å circular mesas, it is important to note that some circular mesa structures show areas of very high dislocation density, i.e., bundles of tightly spaced dislocations. These groups can be seen in Figs. 12(a) and 12(b), which are CL images of 90- and 67- μm mesas, respectively. Such mesas were excluded from the mesa statistics since CL cannot be accurately used to measure such a high density of dislocations.

Figures 13(a)–13(c) are graphs of the linear interface-dislocation density versus mesa size for the samples with 7000 Å of $\text{In}_x\text{Ga}_{1-x}\text{As}$ on 1.5×10^5 -, 10^4 -, and 10^2-cm^{-2} substrates, respectively. The intended composition in all cases was $x = 0.05$, but as shown in Table I, the actual In compositions of the films were $x = 0.05$, 0.095, and 0.05. The general observations are as follows: (1) a decrease in

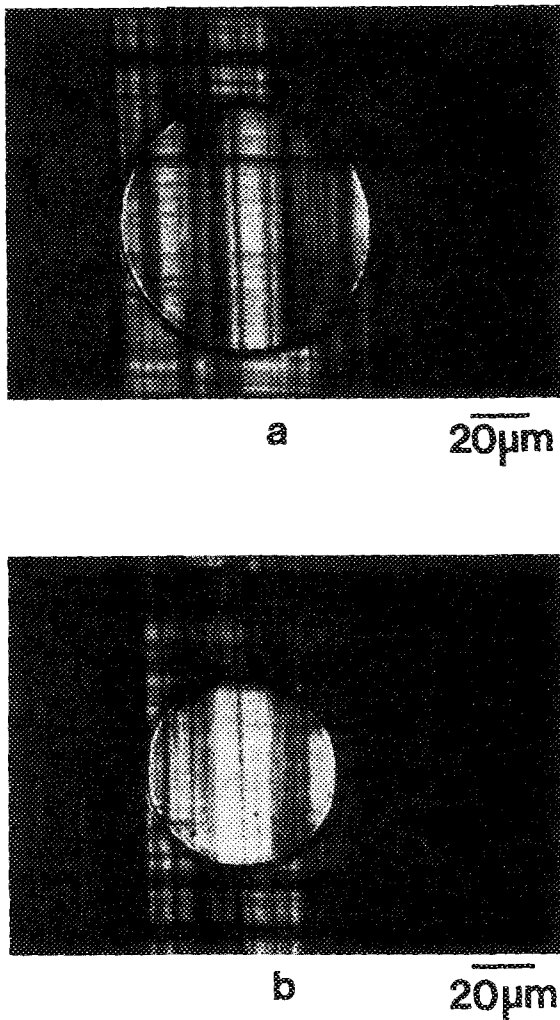


FIG. 12. CL images of mesa structures which have nucleated many dislocations from the mesa edges, forming groups of dislocations: (a) 90- μm circular mesa; (b) 67- μm circular mesa.

linear interface-dislocation density with mesa size; (2) a difference in linear interface-dislocation densities along the two $\langle 110 \rangle$ directions; (3) a linear dependence of linear interface-dislocation density on mesa size for mesas $< 110\text{--}200\ \mu\text{m}$ in diameter; (4) the linear fit to the $[110]$ (solid line) data does not extrapolate through the origin; (5) the slope of the linear fit to the $[110]$ data is independent of substrate dislocation density; and (6) interface-dislocation densities are too high to count for mesas $> 200\ \mu\text{m}$. Observations 1–3 are identical to those previously cited for the 3500- \AA -thick overlayers, but observations 4–6 are unique to the 7000- \AA layer samples. Observations 4–6, along with Figs. 11 and 12, suggest the occurrence of heterogeneous surface half-loop nucleation at mesa edges and will be discussed in Sec. IV.

2. Square mesas

Figures 14(a)–14(d) are CL images of 7000- \AA $\text{In}_{0.05}\text{Ga}_{0.95}\text{As}$ on GaAs square mesas patterned on $1.5 \times 10^5\ \text{cm}^{-2}$ GaAs substrates. The mesas shown in Fig. 14 are from the same samples as the circular mesas in Fig. 11. Figures

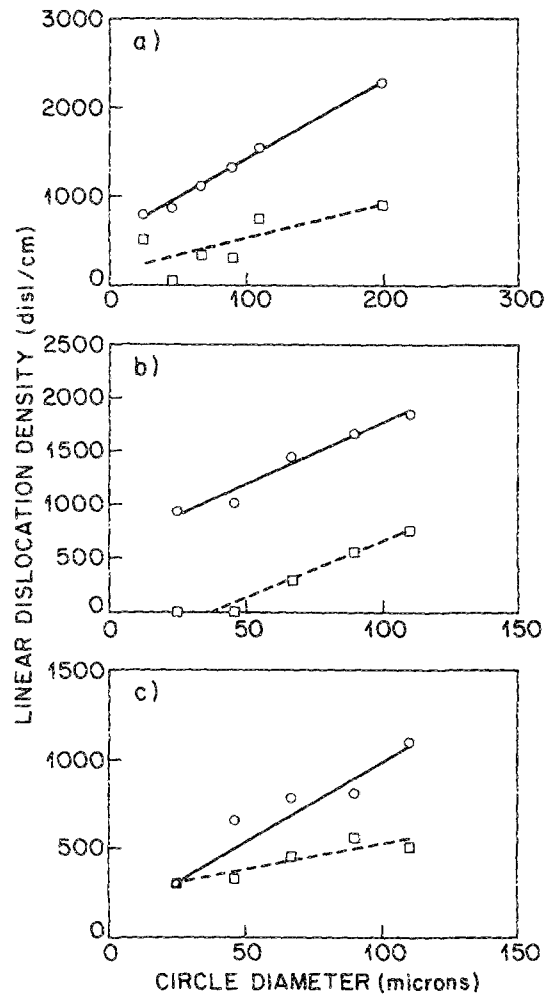


FIG. 13. Plots of average linear interface-dislocation density vs circular mesa diameter for the 7000- \AA $\approx \text{In}_{0.05}\text{Ga}_{0.95}\text{As}$ layers. The solid line represents the dense $\langle 110 \rangle$ direction (defined as $[110]$): (a) $1.5 \times 10^5\text{-cm}^{-2}$ substrate; (b) 10^4-cm^{-2} substrate; (c) 10^2-cm^{-2} substrate.

14(a)–14(d) illustrate the reduction in interface-dislocation density as the mesa size decreases from 400 to 67 μm . Layers grown on mesas in 10^4- and 10^2-cm^{-2} substrates (not shown) were of similar quality and showed the same trends.

Figures 15(a)–15(c) are plots of the linear interface-dislocation density as a function of square mesa edge length. Because the interface-dislocation density in mesas overgrown with 7000 \AA of InGaAs varies greatly, the data points, in spite of averaging, are more scattered than for the 3500- \AA case. Despite the scatter, the same six observations listed for the 7000- \AA circular mesas still hold for the square mesas.

However, one important difference between the circular and square mesas is the number of mesas that exhibit breakdown at the edges, forming bands of dislocations (Fig. 12). Square mesas show a small amount of breakdown at mesa edges, and very few mesas had to be eliminated from the statistics. This is an important point to remember since the circular mesas may appear superior in the edited linear interface-dislocation density graphs.

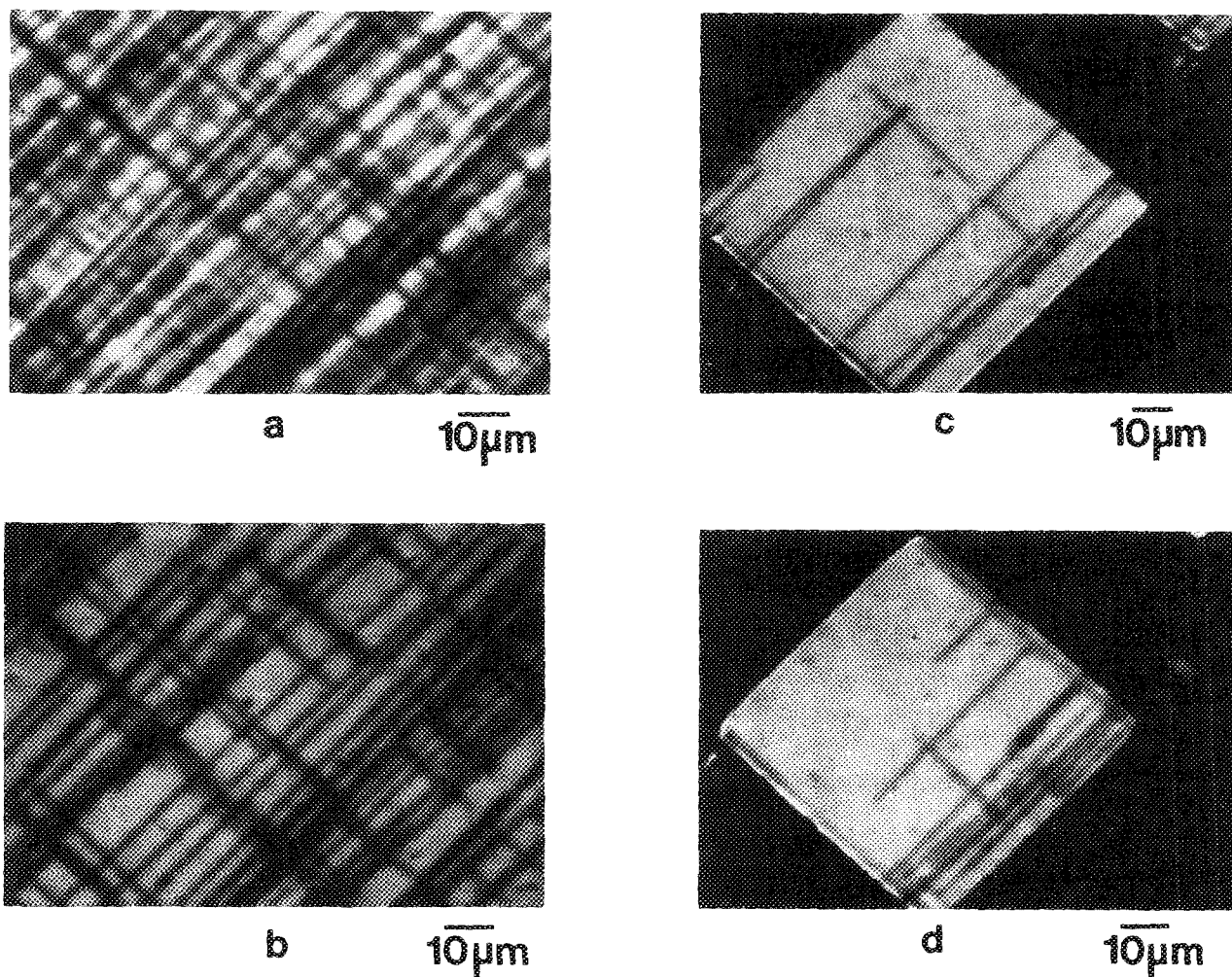


FIG. 14. CL images of the 7000-Å $\text{In}_{0.05}\text{Ga}_{0.95}\text{As}$ layer on the $1.5 \times 10^5\text{-cm}^{-2}$ substrate: (a) 400- μm square mesa; (b) 200- μm square mesa; (c) 90- μm square mesa; (d) 67- μm square mesa.

C. 8250-Å $\text{In}_{0.05}\text{Ga}_{0.95}\text{As}$

We now discuss the results obtained from 8250-Å thick $\text{In}_{0.05}\text{Ga}_{0.95}\text{As}$ layers grown on patterned GaAs substrates with a dislocation density of $1.5 \times 10^5\text{ cm}^{-2}$. At this thickness, the epilayer exceeds the measured large-area critical thickness by more than a factor of 11.

Circular and square mesas: CL images from the circular and square mesas were very similar for these very thick layers. Figures 16(a)–16(c) are CL images from circular mesas with diameters of 400, 110, and 67 μm . On all the different size mesas, the interface-dislocation density was too high to measure with CL. As can be seen in Figs. 16(a)–16(c), the interface-dislocation density in some areas of the interface does decrease, but the density remains high. Because of the inability to count dislocations quantitatively with CL, we measured the CL intensity as a function of island size as a qualitative indication of the number of recombination sites present. After averaging the results from many sets of mesas, we find that the CL intensity increases by approximately 25% as the mesa size decreases from 400 to 25 μm , suggesting a reduction in interface-dislocation density.

IV. DISCUSSION

A. Misfit dislocation sources

Much of the previous work involving the formation of misfit dislocations focused on the energy (or force) balance between the creation of misfit dislocations (considered to occur at the interface only) and strain relief by the misfit dislocation formation.^{11,13–19} However, as mentioned in the Introduction, previous experimental critical thicknesses can generally exceed the theoretical critical thickness calculated in this manner, and the interface-dislocation densities observed in specimens grown beyond the critical thickness are much lower than expected from theory. These facts suggest the presence of a barrier to misfit dislocation nucleation not included in the critical thickness calculations using only strain and dislocation line force or energy.¹² Therefore, understanding the mechanisms of misfit dislocation interactions and nucleation as well as the kinetics of dislocation motion is critical to understanding the final defect morphology in the heterostructure.

As background for the discussion of the effect of area on linear interface-dislocation densities, we first discuss the

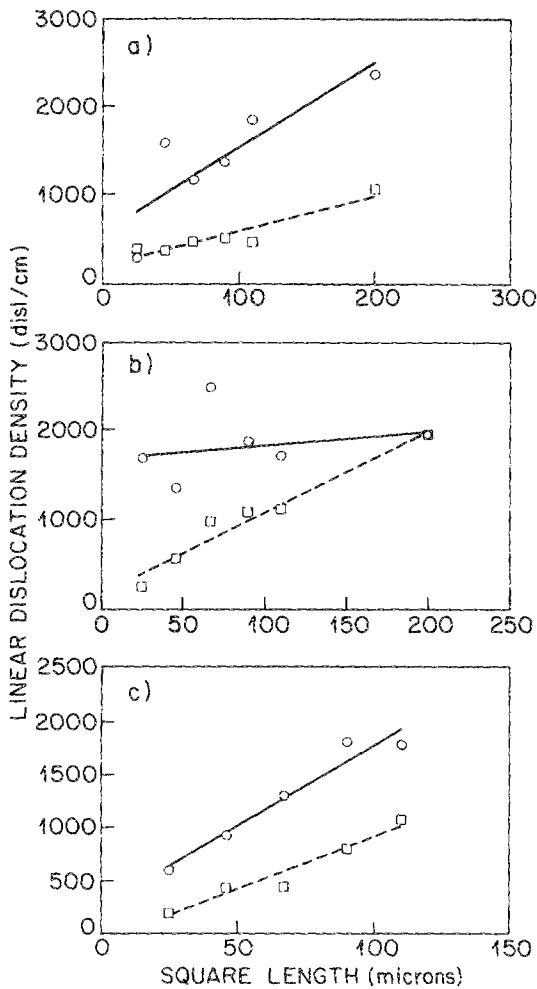


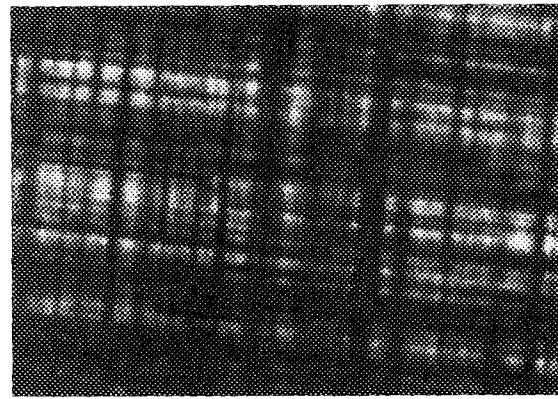
FIG. 15. Plots of average linear interface-dislocation density vs square mesa edge length for the $7000\text{-\AA} \approx \text{In}_{0.05}\text{Ga}_{0.95}\text{As}$ layers. The solid line represents the dense (110) direction (defined as $[110]$): (a) $1.5 \times 10^5\text{-cm}^{-2}$ substrate; (b) 10^4-cm^{-2} substrate; (c) 10^3-cm^{-2} substrate.

three general categories of misfit dislocation nucleation; fixed sources, dislocation multiplication, and surface half-loop nucleation.

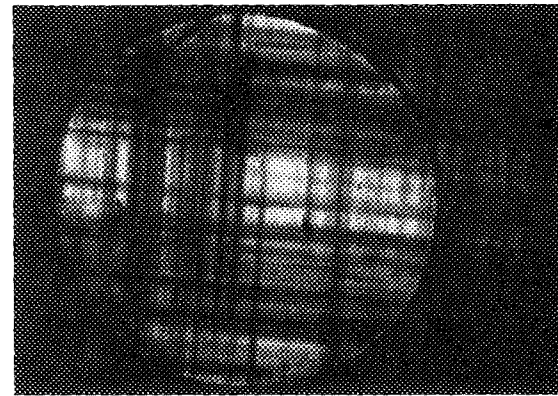
1. Fixed nucleation sources

We define fixed nucleation sources as those sources which decrease linearly in number with a decrease in growth area. Examples of fixed sources are substrate dislocations and substrate surface inhomogeneities.

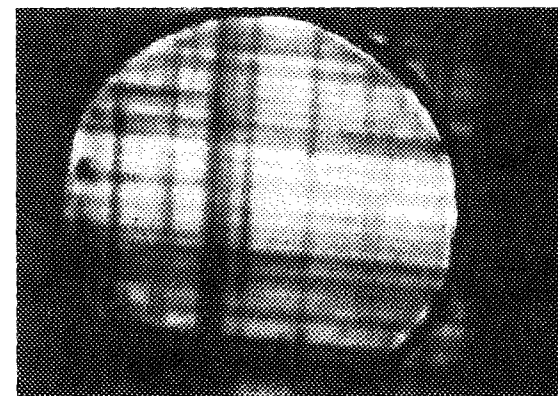
Consider a substrate material which has a certain density of substrate dislocations which intercept the substrate surface. One such dislocation is shown as A in Fig. 17. As a mismatched material is deposited, eventually the strain in the overlayer causes the force on A to become greater than zero, and the threading dislocation segment in the overlayer glides laterally, creating a misfit dislocation at the interface. This defines the critical thickness, the point where the energy to create the misfit dislocation at the interface balances the elastic energy released by the glide of the threading dislocation. The details of calculating such a critical thickness can be found in Refs. 7, 11, and 12.



a $10\mu\text{m}$



b $10\mu\text{m}$



c $10\mu\text{m}$

FIG. 16. CL images of the $8250\text{-\AA} \text{In}_{0.05}\text{Ga}_{0.95}\text{As}$ layer on the $1.5 \times 10^5\text{-cm}^{-2}$ substrate: (a) $400\text{-}\mu\text{m}$ circular mesa; (b) $110\text{-}\mu\text{m}$ circular mesa; (c) $67\text{-}\mu\text{m}$ circular mesa.

We expect fixed sources to have low activation energies for misfit dislocation nucleation since: (1) Threading dislocations already exist in the epilayer as continuations of substrate dislocations, so that nucleation requires only the energy needed to extend the existing misfit dislocation along the

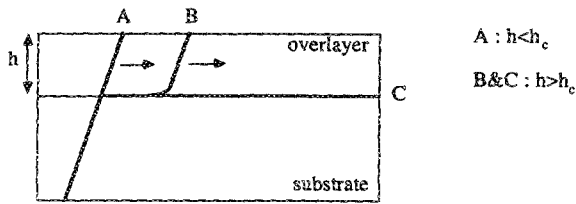


FIG. 17. A schematic diagram showing the generation of a misfit dislocation from a threading dislocation. After the critical thickness, the dislocation in the epilayer glides from A to B and C.

interface. (2) Substrate surface inhomogeneities create large stress concentrations at the heterointerface during growth, thereby drastically reducing the activation energy necessary to heterogeneously nucleate misfit dislocations.

Because of the low activation barriers, we expect that substrate dislocations and substrate surface inhomogeneities are the first nucleation sources to be activated. Therefore, the experimental critical thickness, or the point where misfit dislocations first appear, is usually determined by the fixed nucleation source density. However, films grown on dislocation-free substrates with a low density of surface inhomogeneities will exhibit a critical thickness much larger than expected since it is unlikely that another low-stress source exists in these films. Therefore, the observed critical thickness will be greater and will occur at the stress level corresponding to the next lowest activation energy source (e.g., heterogeneous surface loop nucleation). For example, Si substrates have a high degree of perfection, and the critical thickness for $\text{Ge}_x\text{Se}_{1-x}$ on Si is indeed much larger than predicted by Matthews' theory.¹³

2. Dislocation multiplication and interactions

Once misfit dislocation sources become active, long lengths of misfit dislocations are created. Eventually the misfit dislocations become long enough to ensure a high probability of dislocation interactions.

One type of dislocation interaction is the dislocation multiplication mechanism first described by Hagen and Strunk.⁹ This multiplication is shown schematically in Fig. 18. Figure 18(a) depicts a plan view of a $\{001\}$ interface, with misfit dislocations lying along the $[110]$ and $[\bar{1}\bar{1}0]$ directions. If the dislocations have the same Burgers vector, a repulsive interaction occurs, forming a right-angle segment in the interface and a rounded right-angle segment which lies on a $\{111\}$ plane above the interface plane [Fig. 18(b)]. The $\{111\}$ segment can reach the surface because it is repelled by the junction and because it is attracted to the surface by the surface image force. This mechanism is effective in thin films where the $\{111\}$ segment can reach the surface, creating two new free-ended dislocations [Fig. 18(c)]. These dislocations can now glide and extend the two misfit dislocations to the wafer edge or mesa edge. The remnants of such a reaction produce an intersection as shown in Fig. 18(d). Evidence supporting active Hagen-Strunk mechanisms in the InGaAs/GaAs system has been observed with transmission electron microscopy.¹⁸

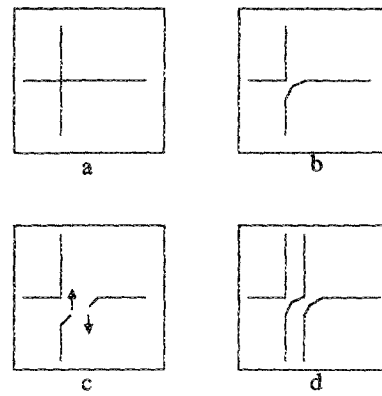


FIG. 18. A schematic diagram which describes dislocation multiplication by the Hagen-Strunk mechanism.

Dislocation multiplication is expected to increase the misfit dislocation density dramatically since two new misfit dislocations are produced for every multiplication event. However, it is unlikely that dislocation multiplication by the Hagen-Strunk mechanism will occur for thick overlayers, since the driving force for the $\{111\}$ segment to reach the specimen surface becomes low as the film thickness increases. Therefore, if Hagen-Strunk multiplication does not occur when the overlayer is thin, a thicker film will not possess interface dislocations generated by this form of multiplication.

We note that other multiplication mechanisms may be active besides that described by Hagen and Strunk. For example, as a misfit dislocation is forming, the dislocation segment extending to the surface may cross other threading segments above the interface plane, i.e., in the epilayer. If the dislocations have the same Burgers vectors, a repulsive reaction will result in a surface half-loop and a segment on a $\{111\}$ plane extending up from the two misfit dislocations in the interface plane. The surface half-loop can grow to form a misfit dislocation at the interface, and the $\{111\}$ segment may glide to the interface region or remain out of the interface plane. It is conceivable that this variation of the Hagen-Strunk multiplication mechanism could occur in thick films when many misfit dislocations are forming.

Dislocation interactions can also lead to an increase in the number of threading dislocations. When active, dislocation multiplication will continually produce large numbers of new gliding threading segments. Many of the threading 60° dislocations will not reach a free edge due to encounters with other dislocations. *In situ* transmission electron microscope observations of misfit dislocation formation show that threading 60° dislocations may be prevented from gliding further due to dislocation interactions at the interface, thereby increasing the density of threading 60° dislocations.²⁰ Also, threading 60° dislocations with appropriate Burgers vectors can react in the epilayer to form a threading sessile edge dislocation. Subsequent strained layers cannot be used to reduce the threading edge dislocation density since the strain cannot move the sessile edge dislocation through the epilayer. The threading edge dislocation is therefore a permanent threading dislocation.

The ideal arrangement of 60° dislocations (in which the

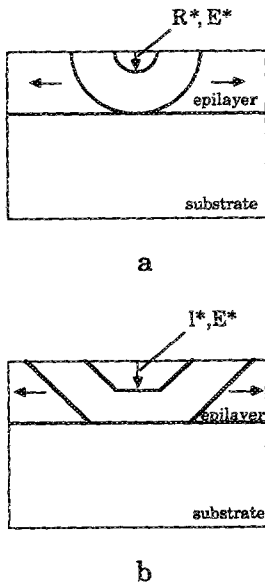


FIG. 19. A schematic diagram showing misfit dislocation formation by surface half-loop nucleation: (a) semicircular loop nucleation; (b) semihexagonal loop nucleation.

screw and tilt components cancel locally) results in the minimum number of dislocations needed to relieve strain.¹⁶ However, because Hagen-Strunk multiplication generates bundles of 60° dislocations with identical Burgers vectors, it is unlikely that the ideal arrangement will form and more 60° dislocations may be present at the interface than the number required for the ideal 60° dislocation distribution.

From the above discussion, it is clearly important to allow misfit dislocations to escape at the edges of the growth area and to limit the glide of dislocations during layer growth in order to prevent dislocation interactions.

3. Surface half-loop nucleation

If the overlayer and substrate have a large lattice mismatch, surface nucleation may occur. As we will show, homogeneous surface nucleation has a large activation energy and the strain required to activate this mechanism is high.

Figure 19(a) depicts the semicircular surface loop nucleation as described by Matthews.²¹ In (001) zinc-blende or diamond heterostructures, surface half-loops nucleate on {111} planes. The activation energy for the formation of this half-loop will be dependent on the strain and surface energy released by the half-loop, as well as the energy needed to create the half-loop. We can approximate the creation energy as one-half the self-energy of a complete circular dislocation loop in an isotropic material²²:

$$E_1 = \frac{Gb^2R}{8} \left(\frac{2-\nu}{1-\nu} \right) \ln \left(\frac{8\alpha R}{e^2b} \right), \quad (1)$$

where G is the shear modulus in the {111} plane, b is the magnitude of the Burgers vector (which is coplanar with the

loop), R is the radius of the loop, ν is Poisson's ratio, and α is the core energy factor (≈ 4 for the diamond cubic lattice²³).

The elastic energy released by the half-loop is found by integrating the force on the dislocation loop over the distance the half-loop has glided:

$$E_e = \int F_e dR, \quad (2)$$

$$F_e = \frac{2G(1+\nu)}{(1-\nu)} \pi R b \epsilon \cos \lambda \cos \phi, \quad (3)$$

where ϵ is the elastic strain in the overlayer, and $\cos \lambda \cos \phi$ resolves the biaxial stress into the glide plane perpendicular to the dislocation line direction. $\cos \lambda$ and $\cos \phi$ are defined by Matthews⁷ and have values of 1/2 and $\sqrt{2/3}$, respectively,¹¹ for 60° dislocations in zinc-blende or diamond crystal structures. Combining Eqs. (2) and (3) gives the strain energy released by the half-loop:

$$E_e = \pi R^2 [Gb(1+\nu)/(1-\nu)] \epsilon \cos \lambda \cos \phi. \quad (4)$$

If we assume a planar growth mode, one atomic layer steps exist on the surface. A surface dislocation half-loop will remove a fraction of the surface steps, thereby releasing surface energy:

$$E_s = 2\gamma b \sin \beta = (Gb^2/4) \sin \beta, \quad (5)$$

where γ is the surface energy per unit area and β is the angle between the Burgers vector and the dislocation line. The right-hand term in Eq. (5) was derived assuming $\gamma = Gb/8$.²¹

The total energy difference of the system due to the formation of the semicircular loop is $E = E_1 - (E_e + E_s)$:

$$E = \frac{GbR}{8(1-\nu)} \left[b(2-\nu) \ln \left(\frac{8\alpha R}{e^2b} \right) - 8\pi R \epsilon (1+\nu) \cos \lambda \cos \phi - 2b(1-\nu) \sin \beta \right]. \quad (6)$$

The critical loop radius for surface nucleation, R^* , can be derived by maximizing Eq. (6) with respect to R :

$$R^* = \frac{b(2-\nu) [\ln(8\alpha R^*/e^2b) + 1] - 2b(1-\nu) \sin \beta}{16\pi \epsilon (1+\nu) \cos \lambda \cos \phi}. \quad (7)$$

If the half-loop grows beyond this critical radius, it will spontaneously grow and reach the interface, eventually forming a misfit dislocation. The activation energy to reach critical radius size is obtained by inserting R^* in Eq. (6), $E^* = E(R^*)$.

The above calculations are for a semicircular loop. However, recent observations suggest a prismatic or semihexagonal geometry for larger loops.²⁴ Using an analogous derivation for the semihexagonal loop shown in Fig. 19(b), we arrive at

$$l^* = \frac{3(2-\nu)b [\ln(4\alpha l^*/c\sqrt{3}b) + 1] - 2\pi b(1-\nu) \sin \beta}{32\pi \epsilon (1+\nu) \cos \lambda \cos \phi}, \quad (8)$$

$$E^* = \frac{\sqrt{3} Gbl^*}{(1-\nu)} \left[\frac{1}{4\pi} (2-\nu) b \ln \left(\frac{4\alpha l^*}{c\sqrt{3}b} \right) - \frac{4}{3} l^* (1+\nu) \epsilon \cos \lambda \cos \phi - \frac{(1-\nu)}{6} b \sin \beta \right], \quad (9)$$

where $c = e^{0.84}$,²⁵ and l^* , the edge length of the hexagon, is analogous to R^* for the semicircular geometry.

Now that we have derived the activation energy necessary for the nucleation of misfit dislocations from the surface, we need to know the energy available for this process under typical growth conditions. According to Matthews,²¹ the available energy for surface nucleation during growth is 50 kT (based on an average loop size), whereas Hirth²⁶ gives 88 kT. Figure 20 shows, for a temperature of 550 °C, the energy necessary to form the different dislocation half-loops as a function of x in $\text{In}_x\text{Ga}_{1-x}\text{As}$ on GaAs. The $\text{In}_x\text{Ga}_{1-x}\text{As}$ elastic constants used in the calculation were calculated by linearly extrapolating between the room-temperature values for InAs and GaAs (i.e., no adjustment was included for the small decrease in the elastic constants between room temperature and the growth temperature).²⁷ The dotted, dotted-dashed, and solid lines are the activation energy curves for a semicircular loop with the core energy factor $\alpha = 1$,²¹ $\alpha \approx 2.718$,²⁶ and $\alpha = 4$.²³ The dashed line is the activation energy curve for a semihexagonal loop with $\alpha = 4$. Also shown is the available thermal energy at 550 °C which, according to above, lies between 50 and 88 kT. Nucleation will occur when the formation energy falls below 50–88 kT. Figure 20 shows that the core energy factor (α) has a large effect on the nucleation point. If $\alpha = 1$, nucleation occurs at $\approx 2\%$ strain, whereas $\alpha = 4$ results in a nucleation point at $\approx 6\%$ strain. Since $\alpha \approx 4$ for diamond cubic lattices, the homogeneous nucleation point will most likely occur when the strain in the overlayer reaches about 6%.

The activation energy curve for the semihexagonal dislocation loop does not intersect the available energy lines, and therefore semihexagonal loops are not likely to nucleate via homogeneous nucleation in the $\text{In}_x\text{Ga}_{1-x}\text{As}/\text{GaAs}$ system. Experimental observations of semihexagonal or prismatic loops can be explained as follows. Semicircular loops will first nucleate due to the lower activation energy. How-

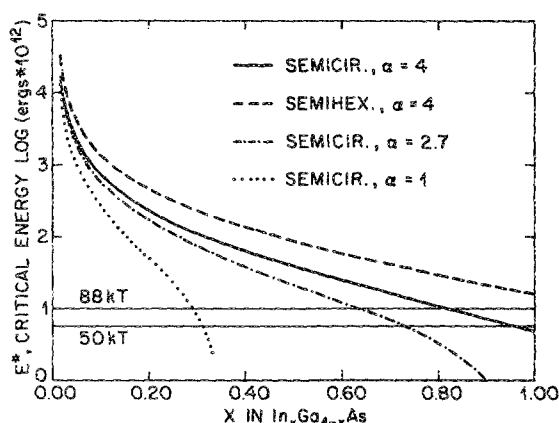


FIG. 20. A plot of the required energy for surface nucleation vs x in $\text{In}_x\text{Ga}_{1-x}\text{As}$ for the $\text{In}_x\text{Ga}_{1-x}\text{As}/\text{GaAs}$ interface. The horizontal lines represent the available energy (50 and 88 kT) during growth for surface nucleation at 550 °C. The curves are the required energy for: dotted = semicircular loop, $\alpha = 1$; dotted-dashed = semicircular loop, $\alpha = e$; solid = semicircular, $\alpha = 4$; dashed = semihexagonal, $\alpha = 4$.

ever, as the loop grows, a substantial image force is present on the end segments.²⁸ This image force results in the rotation of the end segments into the 30° or screw orientation, forming semihexagonal or prismatic loops well after the initial semicircular nucleation.

The surface half-loop calculations show that homogeneous surface nucleation is a high-energy process. It is therefore likely that surface half-loop nucleation first occurs heterogeneously due to edge imperfections or epilayer surface imperfections.

B. The effect of growth area

We now discuss the effect of limiting growth area on the dislocation nucleation sources described above. Figure 21 schematically illustrates the advantages of growth on small areas versus large areas. The black dots represent fixed sources (substrate dislocations and substrate surface inhomogeneities). As a mismatched overlayer is grown on a large area [Fig. 21(a)], misfit dislocations start to nucleate at the many fixed nucleation sites found within the large area, since these have the lowest activation energy of the sources discussed previously. Each of these many nucleation sources can initially form a long misfit dislocation segment since the lateral glide of the dislocation is not inhibited. Long glide and long misfit dislocation lengths result in many dislocation interactions, leading to dislocation multiplication and an increased number of threading dislocations. The new dislocations created by dislocation multiplication can now glide to create even more misfit dislocation length in the interface and more dislocation interactions. The final result is a heterostructure with many threading and interface dislocations.

Now consider growth on small areas, as depicted in Fig. 21(b). As first theorized by Matthews,⁷ a reduction in growth area will reduce the number of threading dislocations available for misfit dislocation formation in that area. This can be shown by considering the definition of the linear interface-dislocation density:

$$\rho_l = 1/S_{l10} = \delta/b_{\text{eff}} = 2\delta/b, \quad (10)$$

where ρ_l is the linear interface dislocation density, S_{l10} is the

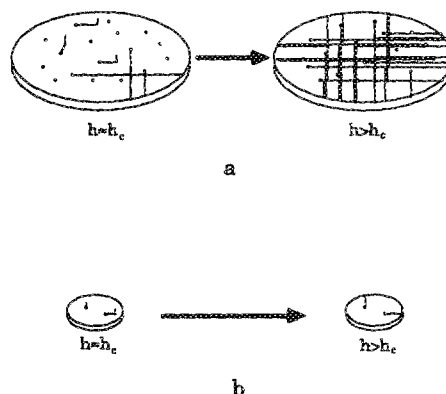


FIG. 21. The formation of interface dislocations for (a) large growth area and (b) small growth area.

dislocation spacing along a $\langle 110 \rangle$ direction, δ is the plastic deformation, b is the Burgers vector, and b_{eff} is the strain relief component of the Burgers vector along one $\langle 110 \rangle$ direction, which is equal to $b/2$ for 60° dislocations. The plastic deformation is

$$\delta = j \rho_f (L/2)(b/2) = j \rho_f L b / 4, \quad (11)$$

where $(b/2)$ is the effective Burgers vector for 60° dislocations for one $\langle 110 \rangle$ direction, ρ_f is the density of fixed nucleation sites (cm^{-2}), $(L/2)$ is an average length of misfit dislocation line in a square growth area of side L , and j is the fraction of fixed nucleation sites which generate misfit dislocations along that $\langle 110 \rangle$ direction. If there is not a difference in $\langle 110 \rangle$ interface-dislocation densities and every fixed nucleation site creates a misfit dislocation, then $j = 1/2$. If 75% of the nucleation sites produce misfit dislocations along a $\langle 110 \rangle$ direction in an asymmetric interface, then $j = 3/4$ for that direction.

Combining Eqs. (10) and (11) yields

$$\rho_l = j \rho_f L / 2. \quad (12)$$

Therefore, if fixed nucleation sources are responsible for all misfit dislocations, the linear interface-dislocation density is proportional to the fixed nucleation site density (ρ_f) and mesa size (L).

For a circular mesa, the derivation is identical, except the average length of a misfit dislocation line in a circular mesa of diameter L is $(\pi/8)L$, giving

$$\rho_l = j \rho_f L \pi / 8. \quad (13)$$

Thus, the number of low activation energy nucleation sites can be reduced by using high-quality substrates and by limiting the size of the growth area. In addition, an operating fixed source cannot generate long lengths of misfit dislocations in the interface due to the escape of the dislocation at the edge of the small growth area. Dislocation interactions are virtually eliminated as well since the average length and lateral glide of misfit dislocations is small, and the probability of dislocation interaction is sharply reduced.

However, homogeneous surface half-loop nucleation will not be affected by a reduction in growth area, since homogeneous surface half-loop nucleation is a function of elastic strain only. As shown above, a high strain is needed for this process. Therefore, if the growth area is reduced and the elastic strain is below $\approx 2\%$ – 6% , very few misfit dislocations will be able to form.

C. Interpretation of results

1. 3500-Å $\text{In}_{0.55}\text{Ga}_{0.95}\text{As}$

Figures 2–7 demonstrate that a large difference exists in linear interface-dislocation densities along the two different $\langle 110 \rangle$ directions in the $[001]$ plane. It is well known that misfit dislocations lying along the two $\langle 110 \rangle$ directions in a (001) plane (termed α and β) have different structure,²⁹ mobility,^{30,31} and electrical properties.³² α dislocations have a higher mobility and lower activation energy to glide than β dislocations, and therefore the dislocations along the dense $\langle 110 \rangle$ direction are likely to be α dislocations. Because we can observe a difference in $\langle 110 \rangle$ interface-dislocation densi-

ties at the very beginning of nucleation, we conclude that α dislocations also nucleate more readily than β dislocations, i.e., the activation barrier is lower for the formation of α dislocations.

The difference in interface-dislocation densities along the two $\langle 110 \rangle$ directions is reflected in Eqs. (12) and (13) by the different values of j for each direction. Using Eqs. (12) or (13), we find that the relationship between the linear interface-dislocation densities from the two $\langle 110 \rangle$ directions gives

$$\frac{\rho_{l_{110}}}{\rho_{l_{\bar{1}\bar{1}0}}} = \frac{m_{110} L_{110}}{m_{\bar{1}\bar{1}0} L_{\bar{1}\bar{1}0}} = \frac{j_{110}}{j_{\bar{1}\bar{1}0}}, \quad (14)$$

where m is the slope of the lines in the ρ_l vs L graphs. Therefore, for square or circular mesas where $L_{110} = L_{\bar{1}\bar{1}0}$, the ratio of the slopes and the fact that $j_{110} + j_{\bar{1}\bar{1}0} = 1$ allows us to calculate the values of j . Using the linear fits from Figs. 4(a)–4(c) and 7(b)–7(c), we arrive at $j_{110} = 0.67$ and $j_{\bar{1}\bar{1}0} = 0.33$. Thus, 2/3 of the fixed nucleation sites result in the nucleation of an α $[110]$ misfit dislocation, whereas 1/3 result in the nucleation of a β $[\bar{1}\bar{1}0]$ misfit dislocation.

As we have stated, Figs. 4, 7, 13, and 15 reveal a linear dependence of the linear interface-dislocation density on mesa size. As shown in the derivation of Eqs. (12) and (13), a linear dependence of ρ_l with L is expected when only fixed sources are active, and therefore the linear dependence is evidence that dislocation multiplication is indeed being blocked. If dislocation multiplication were active, we expect ρ_l to have superlinear dependence on L since two new free-ended dislocations are created for every multiplication event.

Figures 4 and 7 also show that the linear extrapolations nearly pass through zero, within statistical error. This behavior is again expected if only fixed sources are active, as shown by Eqs. (12) and (13) ($L \rightarrow 0$, $\rho_l \rightarrow 0$). If surface nucleation at mesa edges were active, a finite y intercept would exist as the mesa size is extrapolated to zero since part of the linear interface-dislocation density in this case is independent of mesa size, i.e., $\rho_l = j \rho_f L / 2 + \rho_s$, where ρ_s is the linear interface-dislocation density due to surface nucleation. Therefore, surface half-loop nucleation is not an active source, and our choice of $\text{In}_{0.05}\text{Ga}_{0.95}\text{As}$ ($\approx 0.4\%$ strain) is sufficient to halt surface nucleation.

Note also that Figs. 4 and 7 show linear behavior up to the largest mesa size, $400 \mu\text{m}$. This behavior implies an interface-dislocation mean length of at least $200 \mu\text{m}$, since the average interface dislocation length is $L/2$. If the mean length is smaller than $L/2$, Eq. (11) no longer applies. $L/2$ is replaced by the mean length and ρ_l will saturate at a value of $j \rho_f L_{\text{ml}}$, where L_{ml} is the mean length of the dislocation.

If the mean length of the dislocation is equal to or greater than $L/2$ even for large areas, and if only fixed sources are operative, then we can calculate the mesa size at which patterning the substrate no longer has an influence because the dislocation density reaches a value at which the overlayer is completely relaxed. This state will be reached at $L = \rho_l' / m$, where ρ_l' is the linear interface-dislocation density in a completely relaxed heterostructure, and m is the slope of the linear fits in Figs. 4 and 7. As an example, we

TABLE II. Calculated mesa size to achieve complete relaxation. Based on fits to the linear data for the 3500-Å circular mesas in Figs. 4(a) and 4(b).

Substrate dislocation density (cm^{-2})	Interface $\langle 110 \rangle$ direction	Mesa size for 100% relaxation (cm)
1.5×10^5	[110]	2.9
1.5×10^5	[$\bar{1}\bar{1}0$]	6.3
10^4	[110]	8.0
10^4	[$\bar{1}\bar{1}0$]	14.0

have calculated the complete relaxation mesa size for Figs. 4(a) and 4(b), and list the results in Table II. We have assumed an array of 60° dislocations. To calculate the mesa size needed for 50% relaxation, the values in Table II are simply divided by 2.

The calculated mesa sizes for 50%–100% relaxation are large enough such that dislocation interactions are likely; therefore, the mean length will not be equal to $L/2$ in very large mesas and dislocation multiplication and reactions will occur. The mean length can be obtained from future experiments in which the elastic strain, interface-dislocation density, and threading dislocation density are monitored for mesa sizes in the range from $400 \mu\text{m}$ to a few centimeters.

In comparing Figs. 4 and 7, we find that there is little difference between circular and square mesas for 3500 Å, indicating that the geometry or crystallographic orientation of the mesa edges is not critical at this thickness.

By growing on small areas and by growing below the critical strain necessary for surface nucleation, we have eliminated dislocation multiplication and surface nucleation. Therefore, only fixed sources are active, and the linear interface-dislocation density is proportional to mesa size, as expected from Eqs. (12) and (13). Thus, the slope of the lines in Figs. 4 and 7 are representative of the number of fixed nucleation sources (ρ_f). The change in the slopes from the $1.5 \times 10^5 \text{ cm}^{-2}$ substrate sample to the 10^4 cm^{-2} substrate sample indicates a decrease in ρ_f , and the approximately equal slopes of the 10^4 - and 10^2 cm^{-2} substrates suggests an equal ρ_f .

Because only fixed sources are active and nearly every interface dislocation originates from a fixed source, we can use our interface-dislocation density graphs to calculate the number of nucleation sites per unit area. We used both circular and square mesa data for each mesa size in each sample. The results of these calculations are shown in Table III. The number of nucleation sites for the 3500-Å layers decreases from 1.8×10^5 to $4.6 \times 10^4 \text{ cm}^{-2}$ when the substrate dislocation density is reduced from 1.5×10^5 to 10^4 cm^{-2} . The fact that ρ_f falls by a factor of 4 when the substrate dislocation density falls by a factor of 15 suggests a background of non-substrate-dislocation fixed sources of $3.8 \times 10^4 \text{ cm}^{-2}$.

This extra fixed source density is in agreement with the observation that further decreases in substrate dislocation density do not decrease the nucleation site density, i.e., in decreasing the substrate dislocation density from 10^4 to 10^2 cm^{-2} , the nucleation site density remains in the 10^4 cm^{-2} range. Examination of the 10^2 cm^{-2} samples with SEM and

TABLE III. Calculated number of nucleation sites per cm^{-2} .

Thickness (Å)	Substrate dislocation density (cm^{-2})	Nucleation site density (cm^{-2})
3500	1.5×10^5	1.8×10^5
3500	10^4	4.6×10^4
3500	10^2	8.4×10^4
7000	1.5×10^5	2.8×10^5
7000	10^4	3.5×10^5
7000	10^2	2.6×10^5

CL reveals that virtually all of the interface dislocations have originated at substrate surface pits.

Wet chemical etching after the SiO_2 patterns were formed showed that a high density of pinholes existed in the SiO_2 . Therefore, during chemically assisted ion beam etching, small pits are formed on top of the mesas where pinholes exist. When the threading dislocation density from the substrate rises above the $\approx 5 \times 10^4 \text{ cm}^{-2}$ pinhole density, the threading dislocations are the dominant fixed source; if the threading dislocation density from the substrate decreases below the pinhole density, the surface pits generated from the pinholes are now the dominant fixed source. With optimized processing conditions (including the removal of pinholes in the SiO_2 mask), we expect the nucleation site density to track the substrate threading dislocation density until the surface particle density is reached, which will be the limiting nucleation site density.

Note in Table I that the In composition in the 3500-Å, 10^4 cm^{-2} substrate sample was unintentionally 7.5% instead of 5%, yet the interface-dislocation density was insensitive to the higher In composition and remained dependent only on the number of fixed sources. This insensitivity to In composition indicates that surface nucleation is not operative up to 7.5% In, and is further proof that only fixed sources are active.

2. 7000-Å $\text{In}_{0.05}\text{Ga}_{0.95}\text{As}$

When the overlayer thickness is increased to 7000 Å, three new phenomena occur in the linear interface-dislocation density versus mesa size graphs (Figs. 13 and 15): (i) the fit to the [110] data (solid line) does not extrapolate through zero; (ii) there is no consistent change in slope due to different substrate dislocation densities (see Table II also); (iii) and the interface-dislocation densities for mesas greater than 110–200 μm are too high for accurate CL measurements.

The observation that the fit to the [110] data does not extrapolate through zero in Figs. 13 and 15, and that the slopes do not change with substrate dislocation densities, indicates that another source, in addition to the fixed sources, has become active. We represent this source by ρ_s , i.e., ρ_i is now $\rho_i = j\rho_f L/2 + \rho_s$. Table II shows that the nucleation site density is indeed independent of substrate dislocation density. Insight into the type of source can be obtained by examining Figs. 11 and 14. Note that a large number of interface dislocations extend from edge to edge

across the easy α $[110]$ direction as compared to the 3500-Å case. Because the 0.4% strain of the interface is well below the 2%–6% strain necessary for the homogeneous nucleation of surface half-loops as previously calculated, we tentatively identify the nucleation source to be heterogeneous surface nucleation at the mesa edges. Examination of Figs. 13 and 15 shows that the linear interface dislocation density in the $[1\bar{1}0]$ direction (the difficult dislocation formation direction) often tends to go to zero as mesa size decreases to zero. This indicates that the activation energy for heterogeneous surface nucleation has been exceeded in the $[110]$ direction (α dislocations) but not the $[1\bar{1}0]$ direction (β dislocations).

SEM images of the mesas show that a preferential growth of material occurs at the edges, resulting in a rim of greater thickness. This rim also occurs in wafer-size samples and has been shown to nucleate misfit dislocations in the InGaAsP/InP system.^{33–35} We suspect that this thick rim may lower the activation energy necessary to nucleate surface half-loops at the mesa edges. More information about these sources is gained by examining Fig. 12. In circular mesas that exhibit breakdown at the edges, high density dislocation groups extend from non- $\langle 110 \rangle$ parallel edges. The circular mesas have a high density of $\{110\}$ facets when the tangent to the circular mesa edge is not along one of the two $\langle 110 \rangle$ directions in the $[001]$ plane. Therefore, the many edge facets located at 45° to the in-plane $\langle 110 \rangle$ directions either encourage heterogeneous surface nucleation, or the edge faceting increases preferential growth, resulting in a more prominent rim and hence more heterogeneous surface nucleation.

When mesa sizes exceed ≈ 110 – $200 \mu\text{m}$, the interface-dislocation density is too high to be measured reliably with CL. A large increase in interface-dislocation density beyond $200 \mu\text{m}$ may indicate dislocation multiplication. Recall that Hagen–Strunk multiplication requires a thin layer. Because dislocation multiplication via the Hagen–Strunk mechanism does not occur in the 3500-Å layers, it can not occur in the thicker 7000-Å layers. Dislocation multiplication in the 7000-Å layers must occur via dislocation interactions in the epilayer itself, possibly by the modified Hagen–Strunk mechanism postulated in Sec. IV A 2.

For the 7000-Å layers, the linear interface-dislocation density has a linear dependence on mesa size up to $200 \mu\text{m}$. As discussed previously, the linear dislocation density, in the absence of dislocation multiplication, will saturate at a mesa size of twice the mean length. The linear behavior to $\approx 200 \mu\text{m}$ therefore indicates a maximum mean length of $100 \mu\text{m}$. Thus, the mean length of a dislocation in the 7000-Å layer is shorter than the mean length in the 3500-Å layer. This difference in mean length is reasonable, since dislocation interactions are more probable in the 7000-Å layer due to a higher interface-dislocation density.

Note that despite the presence of an additional nucleation source in the 7000-Å samples, the interface-dislocation density is still reduced due to the prevention of many dislocation interactions and the reduction of the number of fixed sources. However, as the mesa size is decreased, the heterogeneous surface half-loop nucleation from the mesa edges

eventually dominates, i.e., $\rho_l \approx \rho_s$, as L goes to zero.

We also point out that despite a doubling in thickness from 3500 to 7000 Å, very little increase in linear interface-dislocation density is observed for mesa sizes below $200 \mu\text{m}$. The relative insensitivity of the linear interface-dislocation density to large changes in thickness indicates the importance of reducing the number of fixed sources and blocking dislocation interactions. If overlayers are grown over large areas, a doubling in epilayer thickness leads to a large increase in interface-dislocation densities.

3. 8250-Å $\text{In}_{0.05}\text{Ga}_{0.95}\text{As}$

Because the density of interface dislocations even in small areas was too high to be accurately measured with CL, our conclusions from the 8250-Å layers are limited. However, the CL intensity does increase by 25% with a decrease in mesa size from 400 to $25 \mu\text{m}$, and regions of mesas are seen to be relatively free of misfit dislocations, indicating that an improvement due to growth area reduction still exists. More recently, we have also observed shifts in the CL emission to higher energies as mesa size is decreased, indicating higher elastic strain and therefore fewer interface dislocations.

V. SUMMARY AND CONCLUSIONS

The effect of a new variable, growth area on strained-layer epitaxy has been investigated. The effect of area on misfit dislocation nucleation sources (fixed, dislocation multiplication, surface nucleation) has been discussed.

3500-Å-thick $\text{In}_{0.05}\text{Ga}_{0.95}\text{As}$ epilayers on GaAs exhibit a linear decrease in linear interface-dislocation density when the mesa width is decreased from 400 to $25 \mu\text{m}$. A 2:1 ratio of linear interface-dislocation densities in the two $\langle 110 \rangle$ directions is observed and attributed to α dislocations nucleating more readily than β dislocations. The linear dependence of the linear interface-dislocation density and the extrapolation through zero when the mesa size decreases to zero indicates that dislocation multiplication and surface nucleation from the mesa edges are not active nucleation sources, and that only fixed sources (ones that scale with area) are active. This is further substantiated by the dependence of the linear interface-dislocation density on substrate dislocation density and surface pits. As long as the mismatch is below that necessary for surface nucleation, and careful processing does not produce a high density of substrate inhomogeneities, the threading dislocation density in the epilayer is therefore reduced.

At 7000 Å, heterogeneous surface nucleation occurs at mesa edges along the easy $[110]$ (α dislocation) direction. The linear interface-dislocation density is linear with mesa size up to $200 \mu\text{m}$, but a large increase in interface-dislocation densities for mesas greater than $200 \mu\text{m}$ may indicate dislocation multiplication in the epilayer. For mesas less than $200 \mu\text{m}$ in width, the linear interface-dislocation density is similar to the density of the 3500-Å layer. This remarkable insensitivity of the interface-dislocation density to thickness further demonstrates the utility of a reduction in growth area.

Mesas with 8250-Å of $\text{In}_{0.05}\text{Ga}_{0.95}\text{As}$ had interface-dislocation densities which were too high to count with CL.

However, increases in CL intensity of about 25% with decreasing mesa size suggest a lower interface-dislocation density on small areas than large growth areas. Therefore, even when surface nucleation occurs, a small growth area decreases the interface-dislocation density and is likely to lower the threading dislocation density by preventing dislocation interactions and by reducing the number of fixed sources.

The linearity of the linear interface-dislocation density with mesa size to greater than 400 μm size mesas in the 3500- \AA -thick samples suggests an interface-dislocation mean length of greater than 200 μm . The linearity in the linear interface-dislocation density in the 7000- \AA -thick samples ends at 200 μm , indicating a maximum mean length of 100 μm . The shorter mean length in the 7000- \AA samples implies a greater number of dislocation interactions.

Fixed sources have the lowest activation energy for misfit dislocation nucleation. Therefore, experimentally observed critical thickness is generally determined by the nucleation of misfit dislocations from fixed sources. If the density of fixed sources is low or zero, then it is unlikely that a nucleation event will occur and be observed. In this case, the experimentally determined critical thickness will be determined by the stress level at which the next lowest activation energy nucleation source becomes active (heterogeneous surface nucleation).

ACKNOWLEDGMENTS

We thank Robert Davis for the chemically assisted ion beam etching of the mesa structures. We gratefully acknowledge support from the Department of Energy under Contract No. DE-FG02-86ER45278, the IBM fellowship program, and the PROSUS programs under the National Nanometer Fabrication Facility at Cornell University. The microscopy facility is operated by the Materials Science Center at Cornell University and supported through a National Science Foundation Grant No. DMR85-16616-AO.

¹J. J. Rosenberg, M. Benlarmi, P. D. Kirchner, J. M. Woodall, and G. D. Pettit, *IEEE Electron Device Lett.* **EDL-6**, 491 (1985).

²L. P. Ramberg, P. M. Enquist, Y.-K. Chen, F. E. Najjar, L. F. Eastman, E. A. Fitzgerald, and K. L. Kavanagh, *J. Appl. Phys.* **61**, 1234 (1987).

- ³S. Katsumoto, A. Yamamoto, and M. Yamaguchi, *Jpn. J. Appl. Phys.* **24**, 636 (1985).
- ⁴T. Tatsumi, H. Hirayama, and N. Aizaki, *Appl. Phys. Lett.* **52**, 895 (1988).
- ⁵G. D. Studtmann, R. L. Gunshor, L. A. Kołodziejcki, M. R. Melloch, J. A. Cooper, Jr., R. F. Pierret, D. P. Munich, C. Choi, and N. Otsuka, *Appl. Phys. Lett.* **52**, 1249 (1988).
- ⁶H. Ito and T. Ishibashi, *Jpn. J. Appl. Phys.* **25**, L421 (1986).
- ⁷J. W. Matthews, S. Mader, and T. B. Light, *J. Appl. Phys.* **41**, 3800 (1970).
- ⁸M. S. Abrahams, L. R. Weisberg, C. J. Buiochi, and J. Blanc, *J. Mater. Sci.* **4**, 223 (1969).
- ⁹W. Hagen and H. Strunk, *Appl. Phys.* **17**, 85 (1978).
- ¹⁰I. J. Fritz, *Appl. Phys. Lett.* **51**, 1080 (1987).
- ¹¹E. A. Fitzgerald and D. G. Ast (unpublished).
- ¹²J. W. Matthews, *J. Vac. Sci. Technol.* **12**, 126 (1975).
- ¹³R. People and J. C. Bean, *Appl. Phys. Lett.* **47**, 322 (1985).
- ¹⁴E. A. Fitzgerald, P. D. Kirchner, R. Proano, G. D. Pettit, J. M. Woodall, and D. G. Ast, *Appl. Phys. Lett.* **52**, 1496 (1988).
- ¹⁵J. Marek, R. Geiss, L. Glassman, and M. Scott, *J. Electrochem. Soc.* **132**, 1502 (1985).
- ¹⁶E. A. Fitzgerald, D. G. Ast, P. D. Kirchner, G. D. Pettit, and J. M. Woodall, *J. Appl. Phys.* **63**, 693 (1988).
- ¹⁷E. A. Fitzgerald, Y. Ashizawa, L. F. Eastman, and D. G. Ast, *J. Appl. Phys.* **63**, 4925 (1988).
- ¹⁸E. A. Fitzgerald, D. G. Ast, Y. Ashizawa, S. Akbar, and L. F. Eastman, *J. Appl. Phys.* **64**, 2473 (1988).
- ¹⁹J. H. Van der Merwe, *J. Appl. Phys.* **34**, 123 (1963).
- ²⁰R. Hull, J. C. Bean, D. J. Werder, and R. E. Leibenguth, *Appl. Phys. Lett.* **52**, 1605 (1988).
- ²¹J. W. Matthews, A. E. Blakeslee, and S. Mader, *Thin Solid Films* **33**, 253 (1976).
- ²²J. P. Hirth and J. Lothe, *Theory of Dislocations*, 2nd ed. (Wiley, New York, 1982), p. 169.
- ²³*ibid.*, p. 231.
- ²⁴E. P. Kvam, D. J. Eaglesham, D. M. Maher, C. J. Humphreys, J. C. Bean, G. S. Green, and B. K. Tanner, *Mater. Res. Soc. Symp. Proc.* **104**, 623 (1988).
- ²⁵J. P. Hirth and J. Lothe, *Theory of Dislocations*, 2nd ed. (Wiley, New York, 1982), p. 170.
- ²⁶J. W. Matthews, *Epitaxial Growth, Part B* (Academic, New York, 1975).
- ²⁷S. Adachi, *J. Appl. Phys.* **53**, 8775 (1982).
- ²⁸J. P. Hirth and J. Lothe, *Theory of Dislocations*, 2nd ed. (Wiley, New York, 1982), p. 151.
- ²⁹M. S. Abrahams, J. Blanc, and C. J. Buiochi, *Appl. Phys. Lett.* **21**, 185 (1972).
- ³⁰H. Steinhardt and P. Haasen, *Phys. Status Solidi A* **49**, 93 (1978).
- ³¹S. A. Erofeeva and Y. A. Osip'yan, *Sov. Phys. Solid State* **15**, 538 (1973).
- ³²A. L. Esquivel, S. Sen, and W. N. Lin, *J. Appl. Phys.* **47**, 2588 (1976).
- ³³S. Yamazaki, Y. Kishi, K. Nakajima, A. Yamaguchi, and K. Akita, *J. Appl. Phys.* **53**, 4761 (1982).
- ³⁴S. Komiya, S. Yamazaki, Y. Kishi, I. Umebu, and T. Kotani, *J. Cryst. Growth* **61**, 362 (1983).
- ³⁵S. Yamazaki, K. Nakajima, S. Komiya, Y. Kishi, and K. Akita, *J. Appl. Phys.* **55**, 3478 (1984).